

University of Wisconsin - Madison

MADPH-98-1057

KEK-TH-589

August 1998

## Searching for $H \rightarrow \tau\tau$ in weak boson fusion at the LHC

D. Rainwater and D. Zeppenfeld

*Department of Physics, University of Wisconsin, Madison, WI 53706*

K. Hagiwara

*Theory Group, KEK, Tsukuba, Ibaraki 305-0801, Japan*

### Abstract

Weak boson fusion is a copious source of intermediate mass Higgs bosons at the LHC. The additional very energetic forward jets in these events provide for powerful background suppression tools. We analyze the  $H \rightarrow \tau\tau$  decay mode for the Standard Model Higgs boson. A parton level analysis of the dominant physics backgrounds (mainly  $Z \rightarrow \tau\tau$  and Drell-Yan production of  $\tau$ 's) and of reducible backgrounds (from  $W$ + jet and  $b\bar{b}$  production in association with two jets and subsequent leptonic decays) demonstrates that this channel allows the observation of  $H \rightarrow \tau\tau$  in a low background environment, yielding a significant Higgs signal with an integrated luminosity of about  $30 \text{ fb}^{-1}$ . The weak boson fusion process thus allows direct measurement of the  $H\tau\tau$  coupling.

## I. INTRODUCTION

The search for the Higgs boson and, hence, for the origin of electroweak symmetry breaking and fermion mass generation, remains one of the premier tasks of present and future high energy physics experiments. Fits to precision electroweak (EW) data have for some time suggested a relatively small Higgs boson mass, of order 100 GeV [1]. This is one of the reasons why the search for an intermediate mass Higgs boson is particularly important [2]. Beyond the reach of LEP at CERN and of the Fermilab Tevatron, for masses in the 110 – 150 GeV range, we show that observation of the  $H \rightarrow \tau\tau$  decay channel at the CERN Large Hadron Collider (LHC) is quite promising. An advantage of the  $H \rightarrow \tau\tau$  channel, in particular compared to the dominant  $H \rightarrow b\bar{b}$  mode, is the lower background from QCD processes. The  $H \rightarrow \tau\tau$  channel thus offers the best prospects for a direct measurement of the Higgs boson's couplings to fermions.

For the intermediate mass range, most of the literature has focussed on Higgs production via gluon fusion [2] and  $t\bar{t}H$  [3] or  $WH(ZH)$  [4] associated production. Cross sections for Higgs production at the LHC are well-known [2], and while production via gluon fusion has the largest cross section by almost one order of magnitude, there are substantial QCD backgrounds but few handles to distinguish them from the signal. Essentially, only the decay products' transverse momentum and the resonance in their invariant mass distribution can be used. The second largest production cross section for the standard model (SM) Higgs boson is predicted for weak-boson fusion (WBF),  $qq \rightarrow qqVV \rightarrow qqH$ . WBF events contain additional information in the observable quark jets. Techniques like forward jet tagging [5–7] can then be exploited to reduce the backgrounds.

Another feature of the WBF signal is the lack of color exchange between the initial-state quarks. Color coherence between initial- and final-state gluon bremsstrahlung leads to suppressed hadron production in the central region, between the two tagging-jet candidates of the signal [8]. This is in contrast to most background processes, which typically involve color exchange in the  $t$ -channel and thus lead to enhanced hadronic activity in the central region. We exploit these features, via a veto on additional soft jet activity in the central region [9].

While some attention has been given to  $A/H \rightarrow \tau\tau$  searches at the LHC [10–12] in the framework of the MSSM, where the increased couplings of  $A/H$  to  $\tau$  predicted for  $\tan\beta \gg 1$  lead to higher production rates, conventional wisdom says that the chance of seeing the SM Higgs via this decay mode is nil, and it has heretofore been ignored in the literature. Thus, we provide a first analysis of intermediate-mass SM  $H \rightarrow \tau\tau$  at the LHC (and of the main physics and reducible backgrounds) which demonstrates the feasibility of Higgs boson detection in this channel, with modest luminosity.  $H \rightarrow \tau\tau$  event characteristics are analyzed for one  $\tau$  decaying leptonically and the other decaying hadronically, because of the high trigger efficiency and good branching ratio of this mode; Ref. [10] found the dual leptonic decay mode to be considerably more difficult due to higher backgrounds.

Our analysis is a parton-level Monte Carlo study, using full tree-level matrix elements for the weak boson fusion Higgs signal and the various backgrounds. In Section II we describe our calculational tools, the methods employed in the simulation of the various processes, and important parameters. Extra minijet activity is simulated by adding the emission of one extra parton to the basic signal and background processes. Generically we call the basic signal process (with its two forward tagging jets) and the corresponding background calculations “2-jet” programs, and refer to the simulations with one extra parton as “3-jet” programs. In Sections III & IV, using the 2-jet programs for physics and reducible backgrounds, respectively, we demonstrate forward jet tagging and  $\tau$  identification and reconstruction criteria which yield an  $\approx 1/1$  signal-to-background (S/B) ratio. Both the  $Wj + jj$  and  $b\bar{b}jj$  reducible backgrounds intrinsically are much larger than the  $Z \rightarrow \tau\tau$  and Drell-Yan  $\tau$ -pair production backgrounds. We explain and emphasize the cuts crucial to reducing these backgrounds to a manageable level.

In Section V we analyze the different minijet patterns in signal and background, using the truncated shower approximation (TSA) [13] to regulate the cross sections. By exploiting the two most important characteristics of the extra radiation, its angular distribution and its hardness, the QCD backgrounds can be suppressed substantially by a veto on extra central jet emission. Within the TSA, probabilities are estimated for vetoing signal and background events, and are combined with the production cross sections of the previous section to predict signal and

background rates in Table IV. These rates demonstrate the possibility to extract a very low background  $H \rightarrow \tau\tau$  signal at the LHC.

Our signal selection is not necessarily optimized yet. Additional observables are available to distinguish the signal from background. The final discussion in Section VI includes a survey of distributions which can be used, e.g. in neural-net algorithms, to further improve the signal significance.

## II. CALCULATIONAL TOOLS

We simulate  $pp$  collisions at the CERN LHC,  $\sqrt{s} = 14$  TeV. All signal and background cross sections are determined in terms of full tree level matrix elements for the contributing subprocesses and will be discussed in more detail below.

For all our numerical results we have chosen  $\sin^2\theta_W = 0.2315$ ,  $M_Z = 91.19$  GeV, and  $G_F = 1.16639 \cdot 10^{-5}$  GeV $^{-2}$ , which translates into  $M_W = 79.97$  GeV and  $\alpha(M_Z) = 128.93$  when using the tree-level relations between these input parameters. This value of  $M_W$  is somewhat lower than the current world average of  $\approx 80.35$  GeV. However, this difference has negligible effects on all cross sections, e.g. the  $qq \rightarrow qqH$  signal cross section varies by about 0.5% for these two  $W$  mass values. The tree level relations between the input parameters are kept in order to guarantee electroweak gauge invariance of all amplitudes. For all QCD effects, the running of the strong-coupling constant is evaluated at one-loop order, with  $\alpha_s(M_Z) = 0.118$ . We employ CTEQ4L parton distribution functions [14] throughout. Unless otherwise noted the factorization scale is chosen as  $\mu_f = \min(p_T)$  of the defined jets.

### A. The $qq \rightarrow qqH(g)$ signal process

The signal can be described, at lowest order, by two single-Feynman-diagram processes,  $qq \rightarrow qq(WW, ZZ) \rightarrow qqH$ , i.e.  $WW$  and  $ZZ$  fusion where the weak bosons are emitted from the incoming quarks [15]. From a previous study of  $H \rightarrow \gamma\gamma$  decays in weak boson fusion [16] we know several features of the signal, which we can directly exploit here: the centrally produced

Higgs boson tends to yield central decay products (in this case  $\tau^+\tau^-$ ), and the two quarks enter the detector at large rapidity compared to the  $\tau$ 's and with transverse momenta in the 20 to 80 GeV range, thus leading to two observable forward tagging jets.

For the study of a central jet veto, the emission of at least one extra parton must be simulated. This is achieved by calculating the cross sections for the process  $qq \rightarrow qqHg$ , i.e. weak boson fusion with radiation of an additional gluon, and all crossing related process. These include

$$q\bar{q} \rightarrow q\bar{q}Hg, \quad \bar{q}q \rightarrow \bar{q}qHg, \quad qq \rightarrow qq\bar{q}H, \quad \bar{q}g \rightarrow \bar{q}q\bar{q}H, \quad (1)$$

and can be found in Ref. [17]. For this case with three final state partons, the factorization scale is chosen as  $\mu_f = \min(p_T)$  of the tagging jets and the renormalization scale  $\mu_r$  is set to the transverse momentum of the non-tagging parton (minijet). Different scale choices or different input parameters will, of course, affect our numerical results. Variation of the factorization scale by a factor of two changes the 2-jet cross section in the last column of Table I by  $\leq \pm 10\%$ .

In the following we only consider  $\tau$ -pair decays with one  $\tau$  decaying leptonically,  $\tau \rightarrow e\nu_e\nu_\tau$ ,  $\mu\nu_\mu\nu_\tau$ , and the other decaying hadronically,  $\tau^\pm \rightarrow h^\pm X$ , with a combined branching fraction of 45%. Our analysis critically employs transverse momentum cuts on the charged  $\tau$ -decay products and, hence, some care must be taken to ensure realistic momentum distributions.

Because of its small mass, we simulate the  $\tau$  decays in the collinear approximation. The momentum fraction  $z$  of the charged decay lepton in  $\tau^\pm \rightarrow \ell^\pm\nu_\ell\nu_\tau$  is generated according to the decay distribution

$$\frac{1}{\Gamma_\ell} \frac{d\Gamma_\ell}{dz} = \frac{1}{3}(1-z) \left[ (5+5z-4z^2) + \chi_\tau(1+z-8z^2) \right]. \quad (2)$$

Here  $\chi_\tau$  denotes the chirality of the decaying  $\tau$  (which, for a negative helicity  $\tau^-$  or positive helicity  $\tau^+$ , is given by  $\chi_\tau = -1$  in the collinear limit). Similarly the pion spectrum for  $\tau^\pm \rightarrow \pi^\pm\nu_\tau$  decays is given by

$$\frac{1}{\Gamma_\pi} \frac{d\Gamma_\pi}{dz} \simeq 1 + \chi_\tau(2z-1). \quad (3)$$

Decay distributions for  $\tau \rightarrow \rho\nu_\tau$  and  $\tau \rightarrow a_1\nu_\tau$  are taken from Ref. [18]. We add the decay distributions from the various hadronic decay modes according to their branching ratios. The

vector meson decays are simulated in the narrow width approximation, which is adequate for our purposes. The decay of the Higgs scalar produces  $\tau$ 's of opposite chirality,  $\chi_{\tau^+} = -\chi_{\tau^-}$  and this anti-correlation of the  $\tau^\pm$  polarizations is taken into account.

Positive identification of the hadronic  $\tau^\pm \rightarrow h^\pm X$  decay requires severe cuts on the charged hadron isolation. Possible strategies have been analyzed by Cavalli *et al.* [10] and we base our simulations on their result. Considering hadronic jets of  $E_T > 40$  GeV in the ATLAS detector, they find non-tau rejection factors of 400 or more (see below) while retaining true hadronic  $\tau$  decays with an identification efficiency

$$\epsilon_\tau(\tau \rightarrow \nu + \text{hadrons}) = 0.26 . \quad (4)$$

This estimate includes the requirement of seeing a single charged hadron track, of  $p_T > 2$  GeV, pointing in the  $\tau$  direction, and thus effectively singles out 1-prong  $\tau$  decays. Accordingly, only the 1-prong hadronic branching ratios are considered in our mixture of  $\pi$ ,  $\rho$  and  $a_1$  modes. Since the overall efficiency includes 3-prong events, which have negligible acceptance, the effective efficiency for 1-prong events is larger and taken as 0.34 in the following, which reproduces the overall efficiency of Eq. (4).

## B. The QCD $\tau^+\tau^- + jj(j)$ physics background

Given the H decay signature, the main physics background to our signal  $\tau^+\tau^-jj$  events arises from real emission QCD corrections to the Drell-Yan process  $q\bar{q} \rightarrow (Z, \gamma) \rightarrow \tau^+\tau^-$ . For  $\tau^+\tau^-jj$  events these background processes include [19]

$$qg \rightarrow qg\tau^+\tau^-, \quad qq' \rightarrow qq'\tau^+\tau^-, \quad (5)$$

which are dominated by  $t$ -channel gluon exchange, and all crossing related processes, such as

$$q\bar{q} \rightarrow g\tau^+\tau^-, \quad gg \rightarrow q\bar{q}\tau^+\tau^-. \quad (6)$$

All interference effects between virtual photon and  $Z$ -exchange are included. The  $Z$  component dominates, however, and we call these processes collectively the “QCD  $Zjj$ ” background. The

cross sections for the corresponding  $Z + 3\text{-jet}$  processes, which we need for our modeling of minijet activity in the QCD  $Zjj$  background, have been calculated in Refs. [20–22]. Similar to the treatment of the signal processes, we use a parton-level Monte-Carlo program based on the work of Ref. [21] to model the QCD  $Zjj$  and  $Zjjj$  backgrounds.

The factorization scale is chosen as for the Higgs boson signal. With  $n = 2$  and  $n = 3$  colored partons in the final state, the overall strong-coupling constant factors are taken as  $(\alpha_s)^n = \prod_{i=1}^n \alpha_s(p_{T_i})$ , *i.e.* the transverse momentum of each additional parton is taken as the relevant scale for its production, irrespective of the hardness of the underlying scattering event. This procedure guarantees that the same  $\alpha_s^2$  factors are used for the hard part of a  $Zjj$  event, independent of the number of additional minijets, and at the same time the small scales relevant for soft-gluon emission are implemented.

The momentum distributions for the  $\tau$  decay products are generated as for the Higgs boson signal. Because of the (axial)-vector coupling of the virtual  $Z, \gamma$  to  $\tau$ 's, the produced  $\tau^+$  and  $\tau^-$  have the same chirality. This correlation of the  $\tau$  polarizations is taken into account by calculating individual helicity amplitudes and folding the corresponding cross sections with the appropriate  $\tau^+$  and  $\tau^-$  decay distributions, *i.e.* the full  $\tau$  polarization information is retained in the energy distribution of the  $\tau$  decay products.

### C. The EW $\tau^+\tau^- + jj(j)$ physics background

These backgrounds arise from  $Z$  and  $\gamma$  bremsstrahlung in quark–(anti)quark scattering via  $t$ -channel electroweak boson exchange, with subsequent decay  $Z, \gamma \rightarrow \tau^+\tau^-$ :

$$qq' \rightarrow qq'\tau^+\tau^- \quad (7)$$

Naively, this EW background may be thought of as suppressed compared to the analogous QCD process in Eq. (5). However, the EW background includes electroweak boson fusion,  $VV \rightarrow \tau^+\tau^-$ , either via  $t$ -channel  $\tau/\nu$ -exchange or via  $s$ -channel  $\gamma/Z$ -exchange, and the latter has a momentum and color structure which is identical to the signal and cannot easily be suppressed via cuts.

We use the results of Ref. [23] for our calculation which ignore  $s$ -channel EW boson exchange contributing to  $q\bar{q}$  production, and Pauli interference of identical quarks. When requiring a large rapidity separation between the two quark jets (tagging jets) the resulting large dijet invariant mass severely suppresses any  $s$ -channel processes which might give rise to the dijet pair, and the very different phase space regions of the two scattered quarks make Pauli interference effects small. All charged-current (CC) and neutral-current (NC) subprocesses are included. The CC process dominates over NC exchange, however, mainly because of the larger coupling of the quarks to the  $W$  as compared to photon and  $Z$  interactions. As in the QCD  $Zjj$  case, the  $Z$ -pole dominates the  $\tau^+\tau^-$  invariant mass distribution, so we will refer to these EW processes as the “EW  $Zjj$ ” background.

The  $\tau$  decay distributions are generated in the same way as described above for the Higgs signal. Since the programs of Ref. [23] generate polarization averaged  $\tau^+\tau^-$  cross sections, we have to assume unpolarized  $\tau$ ’s. However, as for the QCD  $Zjj$  background, the  $\tau^+\tau^-$  pair arises from virtual vector boson decay, resulting in a  $\tau^+$  and  $\tau^-$  of the same chirality. This correlation of the  $\tau$  polarizations is taken into account.

In order to determine the minijet activity in the EW  $Zjj$  background we need to evaluate the  $\mathcal{O}(\alpha_s)$  real parton emission corrections. The corresponding  $\mathcal{O}(\alpha^4\alpha_s)$  diagrams for

$$qq' \rightarrow qq'g \tau^+\tau^- , \quad (8)$$

and all crossing related subprocesses, have first been calculated in Ref. [24]. Production of the  $\tau$ -pair via  $Z$  and  $\gamma$  exchange is considered. The factorization and renormalization scales are chosen to be the same as for the  $Hjj$  signal, as this is also a hard EW process.

We have previously examined other scale choices for the  $Z$  backgrounds [24], and found small uncertainties ( $\approx \pm 15\%$ ) for the EW component, while variations for the QCD component reach a factor 1.5. We thus expect the signal and EW  $Zjj$  background cross sections to be fairly well determined at leading order, while the much larger theoretical uncertainty for the QCD  $Zjj$  background emphasizes the need for experimental input.



### D. The QCD $Wj + jj(j)$ reducible background

Reducible backgrounds to  $\tau^+\tau^- \rightarrow \ell^\pm h^\mp p_T$  events can arise from any process with a hard, isolated lepton, missing  $p_T$ , and an additional narrow jet in the final state which can be mistaken as a hadronically decaying  $\tau$ . A primary reducible background thus arises from leptonic  $W$  decays in  $Wj$  events, where additional QCD radiation supplies the two tagging jet candidates. At lowest order we need to consider  $Wj + jj$  production as the hard process, which is very similar to the simulation of the QCD  $Zjjj$  background discussed before, with the bremsstrahlung  $Z$  replaced by a  $W$ .  $W \rightarrow e\nu_e, \mu\nu_\mu$  decays only are considered and are treated as a fake  $\tau$  decaying leptonically. Real leptonic  $\tau$  decays from  $W \rightarrow \tau\nu_\tau \rightarrow \ell\nu_\ell\nu_\tau$  are relatively suppressed by the  $\tau$  leptonic branching ratio of 35% and the severity of the transverse momentum cuts on the softer charged lepton spectrum. They will be ignored in the following.

Two of the jets in  $Wj + jj$  events are identified as tagging jets, and fluctuations of the third into a narrow jet are considered, resembling a hadronically-decaying  $\tau$ . In Ref. [10] the probability for misidentifying a gluon or light-quark jet as a hadronic  $\tau$  decay was estimated as

$$\epsilon_\tau(\text{jet} \rightarrow \text{"}\nu + \text{hadrons"}) = 0.0025, \quad (9)$$

and we assign this probability to each of the final state jets. In each event one of the hard partons is randomly assigned to be the  $\tau$ . As the  $Wj + jj$  events are a QCD background, we use the same factorization and renormalization scales as for the QCD  $Zjjj$  case.

To simulate additional minijet emission, we need to add one more parton to the final state. The code for  $W + 4j$  matrix elements has been available since the work of Berends et al. [25]. Here we use the program developed in Ref. [26], which was generated via MadGraph [27]. Since  $W + 4j$  production produces a six-particle final state, with up to 516 graphs for the most complicated processes, it takes considerable CPU time to obtain good statistics. We modified the MadGraph code to do random helicity summation, speeding up the calculation by approximately a factor of 3 for a given statistical error in the final cross section. As before,  $\alpha_s$  is taken as the geometric mean of  $\alpha_s(p_T)$  factors for each of the partons, including the parton which fakes the hadronic  $\tau$  decay.

## E. The QCD $b\bar{b}jj$ reducible background

The semileptonic decay of  $b$ -quarks provides another source of leptons and neutrinos which can be misidentified as tau decays. Even though  $b$ -quark decays are unlikely to lead to isolated charged leptons and very narrow tau-like jets in a single event, the sheer number of  $b\bar{b}$  pairs produced at the LHC makes them potentially dangerous. Indeed, the analysis of Ref. [10] found that  $b\bar{b}$  pairs lead to a reducible  $\tau^+\tau^-$  background which is similar in size to  $Wj$  production. We therefore study  $b\bar{b}jj$  production as our second reducible background and neglect any other sources like  $t\bar{t}$  events which were shown to give substantially smaller backgrounds to  $\tau^+\tau^-$ -pairs in Ref. [10].

We only consider  $b$ -production events where both  $b$ -quarks have large transverse momentum. In addition, two forward tagging jets will be required as part of the signal event selection. The relevant leading order process therefore is the production of  $b\bar{b}$  pairs in association with two jets, which includes the subprocesses

$$\begin{aligned} gg &\rightarrow b\bar{b}gg \\ qg &\rightarrow b\bar{b}qg \\ q_1q_2 &\rightarrow b\bar{b}q_1q_2. \end{aligned} \tag{10}$$

The exact matrix elements for the  $\mathcal{O}(\alpha_s^4)$  processes are evaluated, including all the crossing related subprocesses, and retaining a finite  $b$ -quark mass [28]. The Pauli interference terms between identical quark flavors in the process  $q_1q_2 \rightarrow b\bar{b}q_1q_2$  are neglected, with little effect in the overall cross section, due to the large differences in the rapidity of the final state partons. The factorization scale is chosen as the smallest transverse energy of the final state partons before the  $b$ -quark decay. The strong coupling constant  $\alpha_s$  is evaluated at the corresponding transverse energy of the final state partons, i.e.,  $\alpha_s^4 = \alpha_s(E_T(b))\alpha_s(E_T(\bar{b}))\alpha_s(p_{T,\text{jet}_1})\alpha_s(p_{T,\text{jet}_2})$ .

The semileptonic decay  $b \rightarrow \ell\nu c$  of one of the  $b$ -quarks is simulated by multiplying the  $b\bar{b}jj$  cross section by a branching ratio factor of 0.395 (corresponding to at least one semileptonic  $b$ -decay to occur) and by implementing a three-body phase space distribution for the decay

momenta. This part of the simulation is performed in order to estimate the effects of the lepton isolation cuts on the transverse momentum distributions of the  $b$ -decay leptons. Since these are kinematic effects we use the lightest meson masses in the simulation and set  $m_b = 5.28$  GeV and  $m_c = 1.87$  GeV. In Ref. [10] a factor 100 reduction of the  $b\bar{b}$  background was found as a result of lepton isolation, requiring  $E_T < 5$  GeV in a cone of radius 0.6 around the charged lepton. In our simulation, after energy smearing of the charm quark jet (see below), we find a reduction factor of 52 due to lepton isolation with a cone of radius 0.7. However, our simulation does not include parton showers or hadronization of the  $b$ -quark, effectively replacing the  $b$ -quark fragmentation function by a delta-function at one, and thus underestimates the effect of lepton isolation cuts on the  $b$ -quark background. To compensate for this, we multiply our  $b\bar{b}jj$  rates by another factor 0.52, thus effectively implementing the factor 100 suppression found by Cavalli *et al.* [10].

In addition to an isolated lepton, the  $b\bar{b}jj$  events must produce a narrow jet which is consistent with a hadronic  $\tau$  decay. This may either be one of the light quark or gluon jets, for which the misidentification probability of 0.25% of Eq. (9) will be used, or it may be the  $b$ -quark jet. In Ref. [10] the probability for misidentifying a  $b$ -quark jet as a hadronic  $\tau$  decay was estimated as

$$\epsilon_\tau(b \rightarrow \nu + \text{hadrons}) \approx 0.0005 . \quad (11)$$

However, due to limited Monte Carlo statistics, this number was based on a single surviving event only. Since we are really interested in an upper bound on the  $b\bar{b}jj$  background we follow the ATLAS proposal [12] instead, and use the upper bound,

$$\epsilon_\tau(b \rightarrow \nu + \text{hadrons}) < 0.0015 , \quad (12)$$

for our analysis. Thus, all our  $b\bar{b}jj$  cross sections, after  $\tau$  identification, should be considered conservative estimates. A more precise analysis of  $b \rightarrow \tau$  misidentification probabilities in the LHC detectors is clearly needed, an analysis which is beyond the scope of the present work.

The purpose of our  $b$ -analysis is to verify that  $b$  semileptonic decays do not overwhelm the signal. The above procedures are adequate for this purpose, since we obtain final  $b\bar{b}jj$  backgrounds (in Table IV) which are at least one order of magnitude smaller than the signal. We do

not calculate additional  $b$  quark backgrounds arising from intrinsic  $b$  contributions (processes like  $gb \rightarrow bggg$ ). The matrix elements for these processes are of the same order ( $\alpha_s^4$ ) as for the  $b\bar{b}jj$  subprocesses discussed above, but they are suppressed in addition by the small  $b$ -quark density in the proton. Also, we do not simulate additional soft gluon emission for the  $b\bar{b}jj$  background. This would require  $b\bar{b} + 3$  jet matrix elements which are not yet available. Rather, in Section V, we assume the probability for extra minijet emission to be the same as for the other reducible QCD background,  $Wj + jj$  production.

## F. Detector resolution

The QCD processes discussed above lead to steeply falling jet transverse momentum distributions. As a result, finite detector resolution can have a sizable effect on cross sections. Resolution effects are particularly pronounced for the  $b\bar{b}jj$  background, where a higher momentum charm quark (from  $b \rightarrow c\ell\nu$  decay) can fluctuate below the  $E_T(c) < 5$  GeV isolation requirement of the charged lepton.

These resolution effects are taken into account via Gaussian smearing of the energies of jets and  $b$  and  $\tau$  decay products. Following ATLAS expectations [12] we use resolutions

$$\frac{\Delta E}{E} = \frac{5.2}{E} \oplus \frac{0.16}{\sqrt{E}} \oplus .009, \quad (13)$$

for jets (with individual terms added in quadrature), while for charged leptons we use

$$\frac{\Delta E}{E} = 2\%. \quad (14)$$

In addition, finite detector resolution leads to fake missing transverse momentum in events with hard jets. An ATLAS analysis [10] showed that these effects are well parameterized by a Gaussian distribution of the components of the fake missing transverse momentum vector,  $\vec{\cancel{p}}_T$ , with resolution

$$\sigma(\cancel{p}_x, \cancel{p}_y) = 0.46 \cdot \sqrt{\sum E_{T,had}}, \quad (15)$$

for each component. In our calculations, these fake missing transverse momentum vectors are added linearly to the neutrino momenta.

### III. HIGGS SIGNAL AND REAL $\tau^+\tau^-$ BACKGROUNDS

The  $qq \rightarrow qqH$ ,  $H \rightarrow \tau\tau$  signal is characterized by two forward jets and the  $\tau$  decay products. Before discussing background levels and further details like minijet radiation patterns, we need to identify the search region for these hard  $Hjj$  events. Prior to  $\tau$  identification, the task is identical to the Higgs search in  $qq \rightarrow qqH$ ,  $H \rightarrow \gamma\gamma$  which was considered previously [16]. We can thus adopt the strategy of this earlier analysis and start out by discussing three levels of cuts on the  $qq \rightarrow qqH$ ,  $H \rightarrow \tau\tau$  signal, before considering  $\tau$  decay and  $\tau$  identification. This procedure makes explicit the source of the major signal reduction factors which we will encounter.

The basic acceptance requirements must ensure that the two jets and two  $\tau$ 's are observed inside the detector (within the hadronic and electromagnetic calorimeters, respectively), and are well-separated from each other:

$$\begin{aligned} p_{T_{j(1,2)}} &\geq 40, 20 \text{ GeV}, & |\eta_j| &\leq 5.0, & \Delta R_{jj} &\geq 0.7, \\ |\eta_\tau| &\leq 2.5, & \Delta R_{j\tau} &\geq 0.7, & \Delta R_{\tau\tau} &\geq 0.7. \end{aligned} \quad (16)$$

Slightly more than half of all signal events pass these basic cuts. The staggered  $p_{T_j}$  cuts anticipate the steeply falling transverse momentum distributions of both jets for the QCD backgrounds, which are dominated by bremsstrahlung gluons. In contrast, for the  $Hjj$  signal, the  $p_T$  scale is set by the mass of the exchanged weak bosons and most of the tagging jets survive these cuts.

Another feature of the irreducible QCD background is the generally higher rapidity of the  $\tau$ 's as compared to the Higgs signal:  $Z$  and  $\gamma$  bremsstrahlung occur at small angles with respect to the parent quarks, producing  $\tau$ 's forward of the jets. Thus, at the second level of cuts we require both  $\tau$ 's to lie between the jets with a separation in pseudorapidity  $\Delta\eta_{j,\tau} > 0.7$ , and the jets to occupy opposite hemispheres:

$$\eta_{j,min} + 0.7 < \eta_{\tau_{1,2}} < \eta_{j,max} - 0.7, \quad \eta_{j_1} \cdot \eta_{j_2} < 0 \quad (17)$$

At the third level of cuts, which is also the starting point for our consideration of the various backgrounds, a wide separation in pseudorapidity is required between the two forward tagging jets,

TABLE I. Signal  $H \rightarrow \tau\tau$  branching ratio times cross sections for  $m_H = 120$  GeV  $Hjj$  events in  $pp$  collisions at  $\sqrt{s} = 14$  TeV. Results are given for successive cuts of Eqs. (16-18).

	Eq. 16	+ Eq. 17	+ Eq. 18
$B(H \rightarrow \tau^+\tau^-) \cdot \sigma_{Hjj}$ (fb)	132	77	57.6

$$\Delta\eta_{tags} = |\eta_{j1} - \eta_{j2}| \geq 4.4, \quad (18)$$

leaving a gap of at least 3 units of pseudorapidity in which the  $\tau$ 's can be observed. This technique to separate weak boson scattering from various backgrounds is well-established [5–7,9,16], in particular for heavy Higgs boson searches. Table I shows the effect of these cuts on the signal for a SM Higgs boson of mass  $m_H = 120$  GeV. Overall, about 25% of all  $H \rightarrow \tau\tau$  events generated in weak boson fusion are accepted by the cuts of Eqs. (16-18).

The resulting  $Hjj$ ,  $H \rightarrow \tau\tau$  cross section is compared with the irreducible  $Zjj$ ,  $Z \rightarrow \tau\tau$  backgrounds in the first row of Table II. Somewhat surprisingly, the EW  $Zjj$  background reaches 5% of the QCD  $Zjj$  background already at this level, while naively one might expect suppression by a factor  $(\alpha_{QED}/\alpha_s)^2 \approx 4 \times 10^{-3}$ . In the EW  $Zjj$  background,  $W$  exchange processes can produce central  $\tau$  pairs by  $Z$  emission from the exchanged  $W$  and are therefore kinematically similar to the signal. This signal-like component remains after the forward jet tagging cuts, and, as we will see, will grow in relative importance as the overall signal/background ratio is improved.

So far we have not considered  $\tau$  decays. In order to get more realistic rate estimates and to include the reducible backgrounds ( $Wj+jj$  and  $b\bar{b}jj$ , see Section IV) we need to study definite  $\tau$  decay channels. We consider  $\tau^+\tau^-$  decays with one  $\tau$  decaying leptonically ( $e$  or  $\mu$ ) and the other decaying hadronically in the following, since previous studies have shown that dual leptonic decay is more difficult to observe [10]. With a hadronic branching ratio  $B(\tau \rightarrow \nu + \text{hadrons}) = 0.65$  and the overall hadronic  $\tau$ -decay identification efficiency of Eq. (4), the selection of this  $\tau$ -pair decay channel immediately reduces all  $\tau^+\tau^-$  rates by a factor

$$\begin{aligned} \epsilon B &= 2\epsilon_\tau(\tau \rightarrow \nu + \text{hadrons}) B(\tau \rightarrow \nu + \text{hadrons}) B(\tau \rightarrow \ell\nu_\ell\nu_\tau) \\ &= 2 \cdot 0.26 \cdot 0.65 \cdot 0.35 = 1/8.5. \end{aligned} \quad (19)$$

TABLE II. Signal and background cross sections  $B\sigma$  (fb) for  $m_H = 120$  GeV  $Hjj$  events in  $pp$  collisions at  $\sqrt{s} = 14$  TeV. Results are given after increasingly stringent cuts. The last column gives the ratio of the signal to the background cross sections listed in the previous columns.

	$Hjj$	QCD $Zjj$	EW $Zjj$	$Wj + jj$	$b\bar{b} + jj$	S/B
forward tagging [Eqs. (16,17,18)]	57.6	1670	90			
+ $\tau$ identification [Eq. (20)]	1.79	20.0	1.44	52.8	15.2	1/50
+ $110 < m_{\tau\tau} < 130$ GeV [Eq. (22)]	1.18	0.95	0.07	3.54	1.2	1/5
+ $m_{jj} > 1$ TeV, $m_T(\ell, \not{p}_T) < 30$ GeV [Eqs. (23,24)]	0.62	0.17	0.04	0.21	0.29	1/1.1
+ $x_{\tau_l} < 0.75$ , $x_{\tau_h} < 1.0$ [Eq. (25)]	0.49	0.14	0.03	0.05	0.10	1.5/1

In addition, triggering the event via the isolated  $\tau$ -decay lepton and identifying the hadronic  $\tau$  decay as discussed in Ref. [10] requires sizable transverse momenta for the observable  $\tau$  decay products. In the following we require

$$p_{T\tau,lep} > 20 \text{ GeV} , \quad p_{T\tau,had} > 40 \text{ GeV} , \quad (20)$$

where the second requirement is needed to use the results of Cavalli *et al.* on hadronic  $\tau$  identification. These transverse momentum requirements are quite severe and reduce the Higgs signal by another factor of 3.8. Resulting signal and background cross sections are given in the second row of Table II.

Crucial for further background reduction is the observation that the  $\tau$ -pair invariant mass can be reconstructed from the observable  $\tau$  decay products and the missing transverse momentum vector of the event [29]. Denoting by  $x_{\tau_i}$  the fractions of the parent  $\tau$  energy which each observable decay particle carries, the transverse momentum vectors are related by

$$\vec{p}_T = \left(\frac{1}{x_{\tau_l}} - 1\right) \vec{p}_\ell + \left(\frac{1}{x_{\tau_h}} - 1\right) \vec{p}_h . \quad (21)$$

Here we neglect the  $\tau$  mass and assume that the neutrinos from the  $\tau$  decays are collinear with the charged observables, a condition which is satisfied to an excellent degree because of the high

$\tau$  transverse momenta needed to satisfy Eq. (20). As long as the decay products are not back-to-back, Eq. (21) gives two conditions for  $x_{\tau_i}$  and provides the  $\tau$  momenta as  $\vec{p}_\ell/x_{\tau_\ell}$  and  $\vec{p}_h/x_{\tau_h}$ , respectively. This last condition is met in our case because the  $H$  and  $Z$  bosons are typically produced with high  $p_T$ , on the order of 150 GeV for all processes except the  $b\bar{b}jj$  background (in which case the average  $p_T \approx 85$  GeV is still sufficient).

Mismeasured transverse momenta (smearing effects) can still lead to unphysical solutions for the reconstructed  $\tau$  momenta. In order to avoid these, we impose a cut on the angle between the  $\tau$  decay products and require positivity of the calculated  $x_{\tau_i}$ :

$$\cos \theta_{\tau\tau} > -0.9, \quad x_{\tau_{l,h}} > 0. \quad (22)$$

The resulting  $\tau$ -pair invariant mass resolution is somewhat narrower than the one found in Ref. [10], the  $1\text{-}\sigma$  half-width for the  $H$  peak ranging from about 7 GeV for  $m_H = 110$  GeV to about 10 GeV for  $m_H = 150$  GeV (see Fig. 4 below). This improved resolution is an effect of the higher average  $p_T$  of the underlying process: in our case, the two forward tagging jets from weak boson scattering impart a higher  $p_T$  on the  $H$  or  $Z$  than is the case from QCD radiation in gluon fusion. The smaller  $\tau^+\tau^-$  opening angle then leads to a better  $\tau$  momentum reconstruction via Eq. (21). Given this  $\tau$ -pair mass resolution, we choose  $\pm 10$  GeV mass bins for analyzing the cross sections. Signal and background cross sections in a 20 GeV mass bin centered at 120 GeV, after the reconstruction conditions of Eq. (22), are listed in the third row of Table II. QCD and EW  $Zjj$  backgrounds are reduced by a factor of 20, while about 2/3 of the signal survives the mass reconstruction cuts.

Because the QCD backgrounds typically occur at small invariant masses, we can further reduce them by imposing a cut on the invariant mass of the tagging jets,

$$m_{jj} > 1 \text{ TeV}. \quad (23)$$

Fig. 1 shows the tagging jets' invariant mass distribution for the signal and QCD  $Zjj$  background to illustrate the effect of the cut.



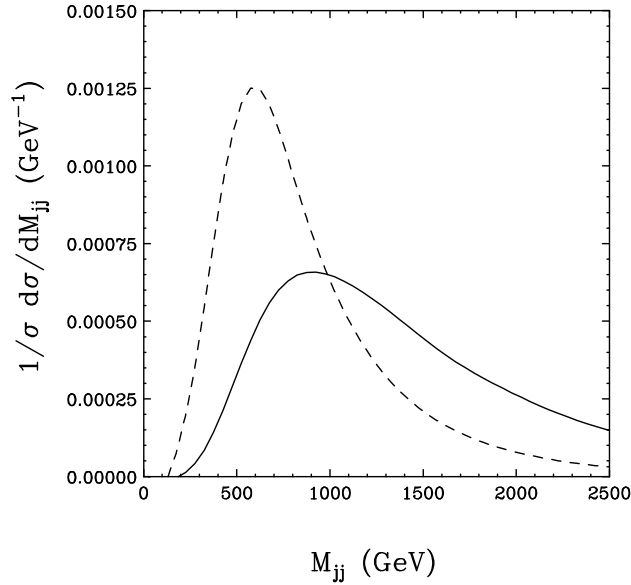


FIG. 1. Invariant mass distribution of the two tagging jets for the  $Hjj$  signal (solid line) and the QCD  $Zjj$  background (dashed line), at the level of forward tagging cuts and  $\tau$  reconstruction, Eqs. (16-22,24).

#### IV. FAKE $\tau^+\tau^-$ EVENTS: REDUCIBLE BACKGROUNDS

Reducible backgrounds to the  $H \rightarrow \tau\tau$  signal, with subsequent leptonic decay of one of the  $\tau$ 's, arise from any source of isolated, single hard leptons. As discussed in Section II, we consider  $Wj + jj$  events and heavy quark production, in the form of  $b\bar{b}jj$  events. Intrinsically, these reducible backgrounds are enormous and overwhelm even the physics backgrounds before  $\tau$  identification and tight lepton isolation cuts are made. Crucial for the reduction of these backgrounds to a manageable level is the requirement of a narrow  $\tau$ -like jet, which leads to a factor 400 suppression for the  $Wj + jj$  background (see Section IID). The probability for a  $b$ -quark to fluctuate into a narrow  $\tau$ -like jet is even smaller, below 0.0015, and another large reduction, by a factor 100 (see Section IIE), is expected from requiring the  $b$ -decay lepton to be well isolated. The resulting background rates, for charged leptons and  $\tau$ -like jets satisfying the transverse momentum requirements of Eq. (20), are listed in the second row of Table II.

Unlike the Higgs signal or the  $Zjj$  backgrounds, the reducible backgrounds show no reso-

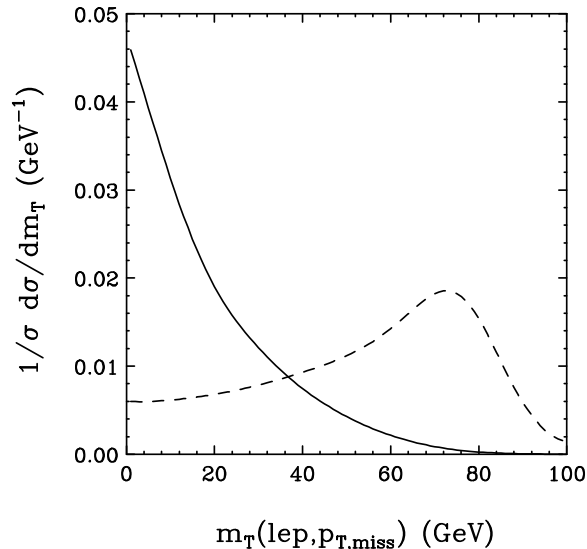


FIG. 2. Transverse mass distribution of the  $\ell\text{-}\cancel{p}_T$  system for the  $Hjj$  signal (solid line) and the  $Wj + jj$  reducible background (dashed line), at the level of far forward tagging cuts,  $\tau$ -reconstruction, and  $m_{jj} > 1$  TeV (Eqs. 16-23).

nance peaks in the  $m_{\tau\tau}$  distribution. As a result, another reduction by an order of magnitude is achieved when comparing rates in a Higgs search bin of width 20 GeV (third row of Table II). Additional reductions are possible by making use of specific properties of the reducible backgrounds. Analogous to the QCD  $Zjj$  background, the  $Wj + jj$  and  $b\bar{b}jj$  backgrounds are created at smaller parton center of mass energies than the signal. As a result, the  $m_{jj} > 1$  TeV cut of Eq. (23) reduces both of them by roughly a factor of 4.

Further suppression of the  $Wj + jj$  background can be achieved by taking advantage of the Jacobian peak in the lepton- $\cancel{p}_T$  transverse mass distribution [10], a feature which is otherwise used to measure the mass of the  $W$ . We compare the  $m_T$  distribution for the signal and the  $Wj + jj$  background in Fig. 2. A cut

$$m_T(\ell, \cancel{p}_T) < 30 \text{ GeV} \quad (24)$$

reduces the  $Wj + jj$  background by a factor of 5 while reducing the signal acceptance by only 15%. Similar to the signal, the other backgrounds are affected very little by the transverse mass cut.

At this level the S/B ratio is nearly 1/1, and we can study additional event characteristics, such as the missing momentum. In real  $\tau$ -pair events, the missing momentum is a vector combination of neutrino momenta, which carry away a significant fraction of the  $\tau^+$  and  $\tau^-$  energies. In the reducible backgrounds it is purely from the leptonically decaying parent particle, either the  $W$  or one of the  $b$ 's. As such, we should reconstruct  $x_{\tau_h} = 1$  for the narrow,  $\tau$ -like jet, except for smearing effects. The effect is clearly observable in the distribution of events in the  $x_{\tau_l}$ - $x_{\tau_h}$  plane, which is shown in Fig. 3. The  $x_{\tau_l}$  distribution of the leptonically decaying  $\tau$ -candidate also is softer for real  $\tau$ 's than for the reducible backgrounds, because the charged lepton shares the parent  $\tau$  energy with two neutrinos. A cut

$$x_{\tau_l} < 0.75, \quad x_{\tau_h} < 1, \quad (25)$$

proves very effective in suppressing the reducible backgrounds. For the  $Wj + jj$  background we find suppression by another factor of 4.5 and the  $b\bar{b}jj$  background is reduced by a factor of 3, while retaining 80% of the signal rate. One should note that these cuts are not optimized, they are merely chosen to demonstrate the usefulness of the  $x_{\tau_l}$ - $x_{\tau_h}$  distributions in restricting the otherwise troublesome reducible backgrounds to a manageable level. Cross sections including these cuts are given in the last row of Table II.

In principle, the  $x_\tau$  distributions contain information on  $\tau$  polarization and  $x_{\tau_l}$ - $x_{\tau_h}$  correlations allow one to distinguish between the decay of a spin-0 object, like the Higgs which results in opposite  $\tau^+$  and  $\tau^-$  chiralities, and the decay of the spin-1  $Z$  boson, with equal  $\tau^\pm$  chiralities [30]. Comparison of the two scatter plots in Fig. (3a) and (3b) shows, however, that the remaining correlations are very weak. This may partially be due to the stringent transverse momentum cuts (20) on the  $\tau$  decay products which needed to be imposed for background reduction. In addition, the visible  $\tau$  energy fractions in  $\tau \rightarrow \ell\bar{\nu}_\ell\nu_\tau$  and  $\tau \rightarrow \rho\nu_\tau$  decays are mediocre polarization analyzers only (measuring the splitting of the  $\rho$ 's energy between its two decay pions would improve the situation for the latter [18]). A dedicated study is needed to decide whether a  $\tau$  polarization analysis is feasible at the LHC, but because of the small rates implied by Table II we do not pursue this issue here.

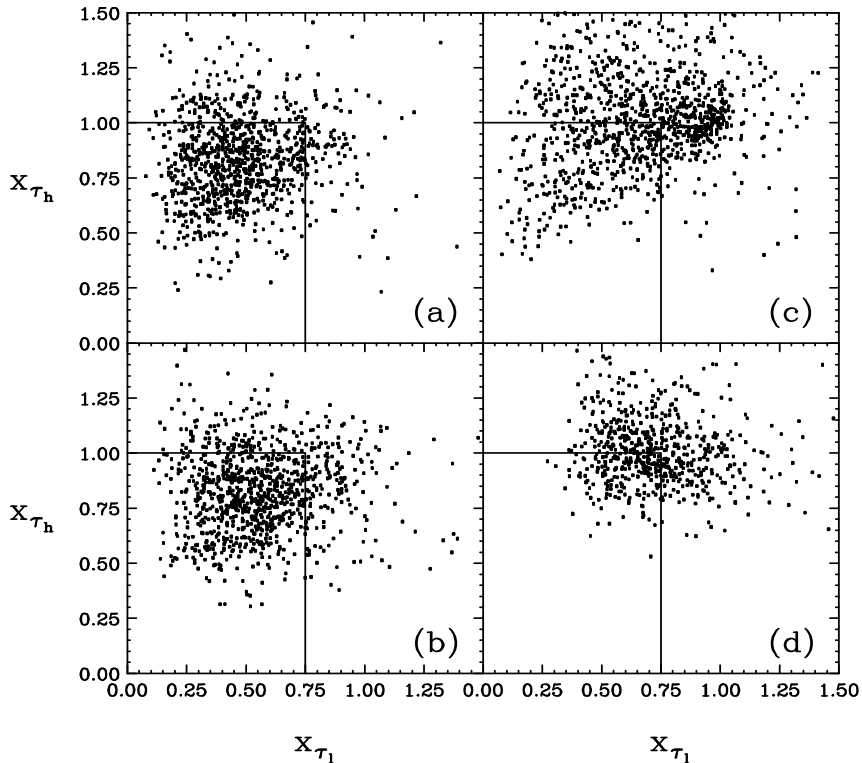


FIG. 3. Scatter plots of  $x_{\tau_l}$  vs.  $x_{\tau_h}$  with the cuts of Eqs.(16-18,20, 22-24), for: (a) the 120 GeV  $Hjj$  signal; (b) the combined QCD and EW  $Zjj$  irreducible backgrounds; (c) the  $Wj + jj$  and (d) the  $b\bar{b}jj$  reducible backgrounds. The number of points in each plot is arbitrary and corresponds to significantly higher integrated luminosities than expected for the LHC. The solid lines indicate the cuts of Eq. (25).

## V. RADIATION PATTERNS OF MINIJETS

A further characteristic of EW vs. QCD scattering can be exploited, namely the absence of color exchange between the two scattering quarks in the  $qq \rightarrow qqH$  signal process.  $t$ -channel color singlet exchange in the EW case leads to soft gluon emission mainly in the very forward and very backward directions, whereas QCD processes are dominated by  $t$ -channel color octet exchange which results in soft gluon radiation mainly in the central detector. It was hoped that resulting rapidity gaps in signal events (large regions in pseudorapidity without observed hadrons) could be used for background suppression [8]. Unfortunately, in  $pp$  collisions of  $\sqrt{s} = 14$  TeV at the LHC, overlapping events in a single bunch crossing will likely fill a rapidity gap even if it is

present at the level of a single  $pp$  collision. Very low luminosity running is not useful because of the small signal cross section.

The different color structures of signal and background processes can be exploited even at high luminosity, however, if one defines rapidity gaps in terms of minijets ( $p_{Tj} \approx 15\text{-}40$  GeV) instead of soft hadrons [9]. As has been shown for the analogous EW  $Zjj$  process [24], with its very similar kinematics, minijet emission in EW exchange occurs mainly in the very forward and very backward regions, and even here is substantially softer than in the QCD  $Zjj$  background. A veto on these central minijets will substantially improve the signal-to-background ratio. Following the analysis of Ref. [24] we veto additional central jets in the region

$$p_{Tj}^{\text{veto}} > p_{T,\text{veto}} , \quad (26a)$$

$$\eta_{j,\text{min}}^{\text{tag}} + 0.7 < \eta_j^{\text{veto}} < \eta_{j,\text{max}}^{\text{tag}} - 0.7 , \quad (26b)$$

where  $p_{T,\text{veto}}$  may be chosen based on the capability of the detector.

Sizable background reduction via a minijet veto requires the lowering of the  $p_{T,\text{veto}}$  threshold to a range where the probability for additional parton emission becomes order unity. In a perturbative calculation the resulting condition,  $\sigma(n+1 \text{ jets}) \approx \sigma(n \text{ jets})$ , indicates that one is leaving the validity range of fixed-order perturbation theory, and it becomes difficult to provide reliable theoretical estimates of minijet emission rates. Gluon emission is governed by very different scales in signal as compared to background processes, due to their different color structures. Thus, a parton shower approach does not immediately give reliable answers unless both color coherence and the choice of scale are implemented correctly, corresponding to the answer given by a complete QCD calculation.

The necessary additional information on angular distributions and hardness of additional radiation is available in the “3 jet” programs discussed in Section II. However, cross sections evaluated with these minijet emission codes exceed the hard-process cross sections at moderate transverse momenta of the additional jet already, namely at  $p_{T,\text{veto}} \approx 40$  GeV for the QCD cases and  $\approx 10$  GeV for the EW cases. In order to extract meaningful estimates, with  $p_{T,\text{veto}} \approx 15 - 20$  GeV, one needs to regulate the  $p_{Tj} \rightarrow 0$  singularities. We use the truncated shower

approximation (TSA) [13] for this purpose, which simulates the effects of soft multiple-gluon emission by replacing the tree-level 3 jet differential cross section,  $d\sigma_3^{\text{TL}}$ , with

$$d\sigma_3^{\text{TSA}} = d\sigma_3^{\text{TL}} \left( 1 - e^{-p_{T3}^2/p_{TSA}^2} \right) . \quad (27)$$

Here the parameter  $p_{TSA}$  is chosen to correctly reproduce the tree-level 2 jet cross section,  $\sigma_2$ , within the cuts of Eqs. (16-18,20, 22-24), *i.e.*  $p_{TSA}$  is fixed by the matching condition

$$\sigma_2 = \int_0^\infty \frac{d\sigma_3^{\text{TSA}}}{dp_{T3}} dp_{T3} . \quad (28)$$

We find  $p_{TSA} = 6.7$  GeV for the  $Hjj$  signal,  $p_{TSA} = 12.1$  GeV for the EW  $Zjj$  background, and  $p_{TSA} = 60$  GeV for the QCD  $Zjj$  and  $Wj + jj$  backgrounds. The much larger value for the QCD processes again reflects the higher intrinsic momentum scale governing soft-gluon emission in the QCD backgrounds. This difference is enhanced even more by requiring larger dijet invariant masses for the two tagging jets [24].

Using  $d\sigma_3^{\text{TSA}}$  as a model for additional jet activity, we can study the efficiency of vetoing central soft jet emission. The survival probability for signal and background processes is found by rejecting events with a minijet of  $p_{Tj}^{\text{veto}} > p_{T,\text{veto}}$  in the gap region (26b), and by dividing the resultant, regulated cross section by the inclusive ( $2j$ ) cross section. Results are summarized in Table III. In order to determine these numbers, we must first select two of the three final state partons as tagging jets, for which several methods exist. In the first, dubbed “ $p_T$ -method”, we choose the two jets with the highest  $p_T$ ’s, because the quark jets of the signal are typically much harder than gluon jets from additional soft radiation. Two other choices, the “R-method” and “ $\eta$ -method”, select the two jets closest to the reconstructed Higgs boson in  $\Delta R$  and  $\Delta\eta$ , respectively, because additional radiation in the signal is mainly expected in the very far forward regions, at larger separations from the Higgs boson than the quark jets. The R- and  $\eta$ -methods give slightly higher signal significances, but are still consistent with the  $p_T$ -method. Results in Table III were derived with the  $\eta$ -method.

The minijet veto reduces the signal by about 30%, but eliminates typically 85% of the QCD backgrounds. The EW  $Zjj$  background is reduced by about 50%, reflecting a radiation pattern

TABLE III. Survival probabilities for the signal and backgrounds, using the  $\eta$ -method for selecting the tagging jets, and for  $p_{T,veto} = 20$  GeV. The second row gives the number of events expected for  $30 \text{ fb}^{-1}$  of integrated luminosity, after application of all cuts, Eqs.(16-18,20, 22-25), and for  $m_H = 120$  GeV and  $110 < m_{\tau\tau} < 130$  GeV. Survival probabilities for the  $b\bar{b}jj$  background are assumed to be the same as for the  $Wj + jj$  background. As a measure of the Poisson probability of the background to fluctuate up to the signal level, the last column gives  $\sigma_{Gauss}$ , the number of Gaussian equivalent standard deviations.

	$Hjj$	QCD $Zjj$	EW $Zjj$	$Wj + jj$	$b\bar{b}jj$	$\sigma_{Gauss}$
$P_{surv}$	0.71	0.14	0.48	0.15	0.15	
no. events	10.4	0.61	0.46	0.21	0.47	4.9

for the  $t$ -channel  $W$ -exchange graphs which is similar to the signal process, but also indicates the presence of additional bremsstrahlung processes which allow radiation back into the central region. In addition, the exchanged transverse  $W$ 's in the EW  $Zjj$  case result in higher- $p_T$  quark jets, on average, than the longitudinal  $W$ 's that are exchanged in the  $Hjj$  signal. This is also reflected in the slightly higher value for  $p_{TSA}$  in the EW  $Zjj$  case as compared to the  $Hjj$  signal.

Table IV applies the survival probabilities found for the  $\eta$ -method to the cross sections after final cuts, for Higgs boson masses ranging from 110 to 150 GeV. A constant size of the mass bins of 20 GeV is kept for simplicity. In the actual experiment, the mass window will need to be optimized depending on the predicted width of the signal and background distributions, and may have to be asymmetric for low values of  $m_H$ . Our table merely shows how observing a light Higgs boson is quite feasible, even in the mass window close to the smeared  $Z$  peak. As  $m_H$  approaches 150 GeV, however, the  $H \rightarrow \tau\tau$  branching ratio drops rapidly in the SM and the signal gets low for integrated luminosities of order  $30 \text{ fb}^{-1}$ . It should be noted that with higher luminosity, this channel is still very effective to make a direct measurement of the  $H\tau\tau$  coupling.

TABLE IV. Number of expected events for the signal and backgrounds, for  $30 \text{ fb}^{-1}$  integrated luminosity and cuts as in Table III, but for a range of Higgs boson masses. Mass bins of  $\pm 10 \text{ GeV}$  around a given central value are assumed.

$m_H(\text{GeV})$	$Hjj$	QCD $Zjj$	EW $Zjj$	$Wj + jj$	$b\bar{b}jj$	$\sigma_{Gauss}$
110	11.1	2.1	1.4	0.2	0.5	4.0
120	10.4	0.6	0.5	0.2	0.5	4.9
130	8.6	0.3	0.3	0.2	0.4	4.7
140	5.8	0.2	0.2	0.2	0.4	3.6
150	3.0	0.1	0.2	0.2	0.3	2.1

## VI. DISCUSSION

The results summarized in Table IV show that it is possible to isolate a virtually background free  $qq \rightarrow qqH$ ,  $H \rightarrow \tau\tau$  signal at the LHC, with sufficiently large counting rate to obtain a  $5\sigma$  signal with a mere  $30 \text{ fb}^{-1}$  of data. The expected purity of the signal is demonstrated in Fig. 4, where the reconstructed  $\tau\tau$  invariant mass distribution for a SM Higgs boson of mass  $120 \text{ GeV}$  is shown, together with the various backgrounds, after application of all cuts discussed in the previous Section. This purity is made possible because the weak boson fusion process, together with the  $H \rightarrow \tau^+\tau^- \rightarrow \ell^\pm \text{hadrons}^\mp \cancel{p}_T$  decay, provides a complex signal, with a multitude of characteristics which distinguish it from the various backgrounds.

The basic feature of the  $qq \rightarrow qqH$  signal is the presence of two forward tagging jets inside the acceptance of the LHC detectors, of sizable  $p_T$ , and of dijet invariant mass in the TeV range. Typical QCD backgrounds, with isolated charged leptons and two hard jets, are much softer. In addition, the QCD backgrounds are dominated by  $Z$  or  $W$  bremsstrahlung off forward scattered quarks, which gives typically higher-rapidity charged leptons (see Fig. 5). In contrast, the EW processes give rise to quite central leptons, and this includes not only the Higgs signal but also EW  $Zjj$  production, which also proceeds via weak boson fusion. It is this similarity that prevents one from ignoring EW  $Zjj$  processes, which a priori are smaller by two orders of magnitude in



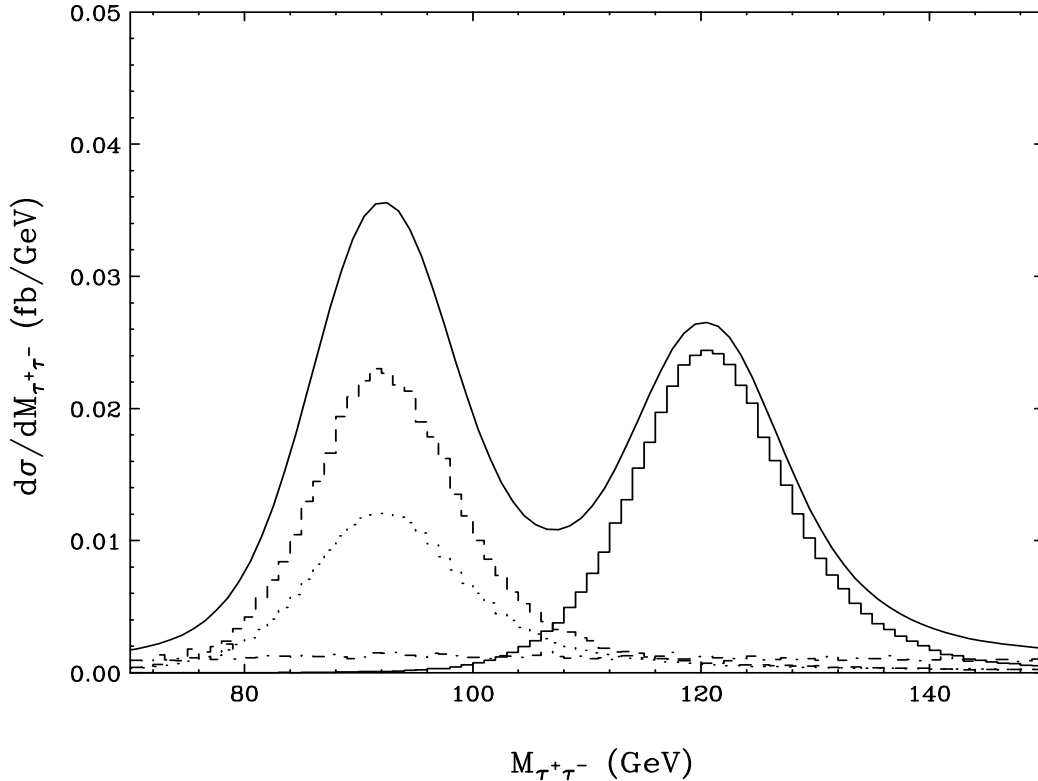


FIG. 4. Reconstructed  $\tau$  pair invariant mass distribution for the signal and backgrounds after the cuts of Eqs. (16-25) and multiplication of the Monte Carlo results by the expected survival probabilities. The solid line represents the sum of the signal and all backgrounds. Individual components are shown as histograms: the  $Hjj$  signal (solid), the irreducible QCD  $Zjj$  background (dashed), the irreducible EW  $Zjj$  background (dotted), and the combined  $Wj + jj$  and  $b\bar{b}jj$  reducible backgrounds (dash-dotted).

total cross section, but after final cuts remain the same size as their QCD counterparts.

We advocate taking advantage of an additional fundamental characteristic of QCD and EW processes. Color-singlet exchange in the  $t$ -channel, as encountered in Higgs boson production by weak boson fusion (and in the EW  $Zjj$  background), leads to additional soft jet activity which differs strikingly from that expected for the QCD backgrounds in both geometry and hardness: gluon radiation in QCD processes is typically both more central and harder than in WBF processes. We exploit this radiation, via a veto on events with central minijets, and expect a typical 85% reduction in QCD backgrounds, but only about a 30% loss of the signal.

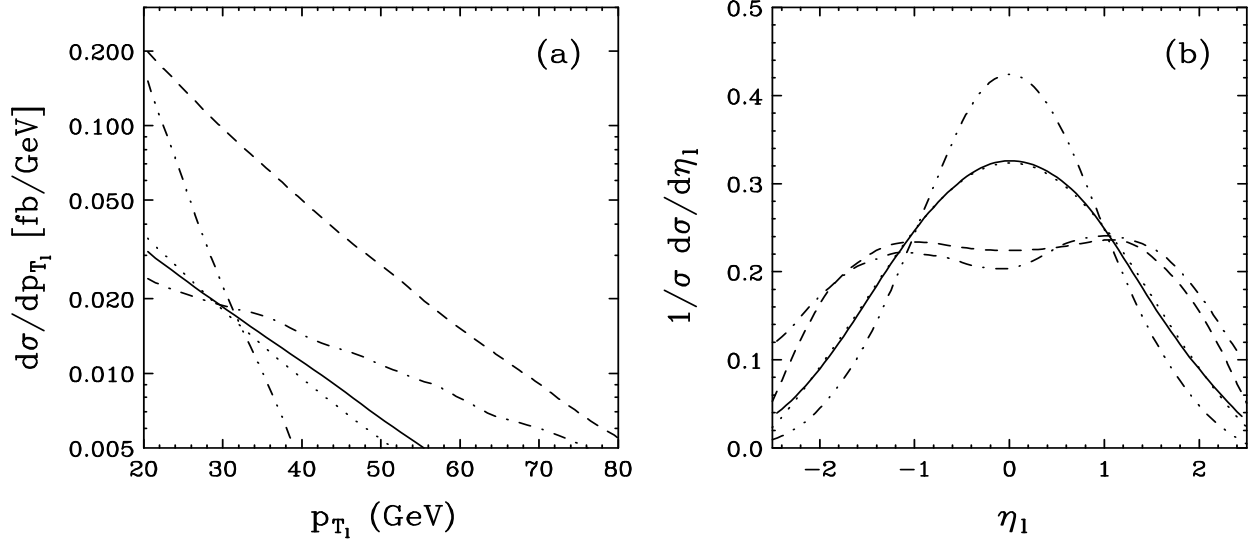


FIG. 5. (a) Transverse momentum and (b) pseudorapidity distributions of the charged “ $\tau$ ” decay lepton for the  $m_H = 120$  GeV signal (solid line), and backgrounds: QCD  $Zjj$  production (dashed line), EW  $Zjj$  events (dotted line),  $Wj+jj$  events (dot-dashed line), and  $b\bar{b}jj$  production (dash-double dotted line).

The properties mentioned so far are generic in the search for weak boson fusion events. Additional cuts are specific to the  $H \rightarrow \tau\tau$  channel, with one  $\tau$  decaying leptonically and the other one decaying hadronically. Crucial are charged lepton isolation and efficient identification of the hadronically decaying  $\tau$ , which are needed for the suppression of heavy quark backgrounds and non- $\tau$  hadronic jets. This part of the analysis we have adapted from Ref. [10], which, however, was performed for  $A, H \rightarrow \tau\tau$  events from gluon fusion, i.e. without requiring two additional forward tagging jets. A more detailed assessment of lepton isolation and hadronic  $\tau$  identification in the present context is beyond the scope of the present work and should be performed with a full detector simulation.

The elimination of the  $Wj+jj$  reducible background highly depends upon the Jacobian peak in the transverse mass distribution of the  $W$  decay products. The other backgrounds and the Higgs signal typically produce rather small values of  $m_T(\ell, \cancel{p}_T)$ , below 30 GeV, and thus well below the peak in  $m_T(W)$ .

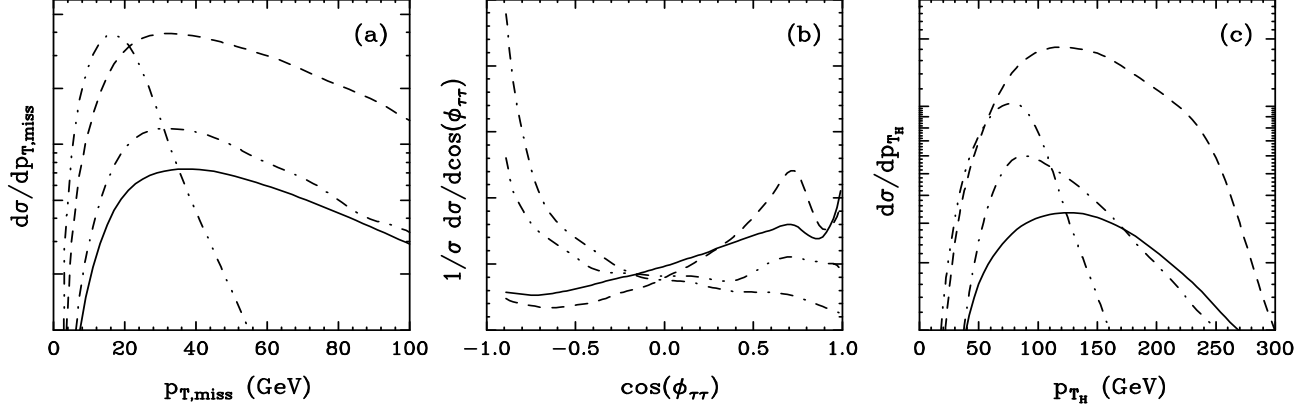


FIG. 6. Shape comparison of various distributions for the Higgs signal (solid line) and the backgrounds: QCD  $Zjj$  production (dashed line),  $Wj + jj$  events (dot-dashed line), and  $b\bar{b}jj$  production (dash-double dotted line). Shown are the (a)  $p_T$ , (b)  $\cos(\phi_{\tau\tau})$  and (c) transverse momentum distribution of the reconstructed  $\tau\tau$  system.

Another distinguishing feature of real  $\tau$  decays are the reconstructed momentum fractions  $x_{\tau_l}$  and  $x_{\tau_h}$  of the charged decay lepton and of the decay hadrons. Misidentified “ $\tau$ ’s” tend to produce unphysically large values for these momentum fractions and can thereby be eliminated to a substantial degree (see Fig. 3). The reconstruction of these  $\tau$  momentum fractions is possible since the  $\tau^+\tau^-$  pairs are typically being produced with sizable transverse momenta (see Fig. 6c)). As a result back-to-back  $\tau^+\tau^-$  decay products are rare (see Fig. 6b)) and this in turns allows the mass reconstruction of the  $\tau$ -pair, which is crucial for the suppression of the main physics background,  $Z \rightarrow \tau\tau$ .

We have not made full use of the differences between the Higgs signal and the various backgrounds in some of these distributions. Additional examples are shown in Figures 5 and 6. Fig. 5 shows the  $p_{T\ell}$  and  $\eta_\ell$  distributions for the observable charged lepton, which will form an important part of the event trigger. As a result of the lepton isolation cut, the  $p_{T\ell}$  falloff is considerably steeper for the  $b\bar{b}jj$  background than for the signal and the other backgrounds. Not much leeway is present in applying more stringent cuts, however, without losing a substantial fraction of the signal. One can also take advantage of the  $\eta_\ell$  distribution for the QCD  $Zjj$  background, which,

at the final level of cuts, remains important in particular for small values of the Higgs boson mass.

In addition to the lepton  $p_T$ , we may use the missing transverse momentum of the event,  $\cancel{p}_T$ , see Fig. 6 (a), which is exceptionally small for the  $b\bar{b}jj$  background. In combination with a more stringent cut on the  $\tau$  pair opening angle,  $\cos(\phi_{\tau\tau})$ , shown in Fig. 6 (b) (where an even more striking distinction between the physics and the reducible processes is found), both the  $Wj + jj$  and  $b\bar{b}jj$  backgrounds can be reduced even below the level discussed in Section V. Such a strategy, however, may not increase the statistical significance of the signal. In fact we find that slightly looser cuts, for example on the dijet invariant mass,  $m_{jj}$ , can somewhat increase the significance of the signal while reducing the signal-to-background ratio. These points demonstrate that we have not yet optimized the search strategy for  $H \rightarrow \tau\tau$  decays. This might be possible by combining the information from all the distributions mentioned above in a neural-net analysis. It is premature at this stage, however, to perform such an analysis since the issues of  $\tau$ -identification or of suppression of heavy quark decays in a realistic detector need to be addressed simultaneously, for the specific processes considered here.

Beyond the possibility of discovery of the Higgs boson in the  $H \rightarrow \tau\tau$  mode, or confirmation of its existence, the independent measurement of the  $H\tau\tau$  coupling will be another important reason to strive for observation of  $H \rightarrow \tau\tau$  decays at the LHC. For such a measurement, via the analysis outlined in this paper,  $\tau$ -identification efficiencies, minijet veto probabilities etc. must be precisely known. For calibration purposes, the presence of the  $Z \rightarrow \tau\tau$  peak in Fig. 4 will be of enormous benefit. The production rates of the QCD and EW  $Zjj$  events can be reliably predicted and, thus, the observation of the  $Z \rightarrow \tau\tau$  peak allows for a direct experimental assessment of the needed efficiencies, in a kinematic configuration which is very similar to the Higgs signal.

Observation of the  $H \rightarrow \tau\tau$  decay mode at the LHC, for the SM Higgs, and for modest integrated luminosities appears to be a real possibility. What is needed is that the Higgs boson lies in the mass range between present LEP limits and about 150 GeV, where its  $\tau\tau$  branching fraction is sizable. In models beyond the SM prospects may be even better. Weak boson fusion at

the LHC will be an exciting process to study at the LHC, for a weakly coupled Higgs sector just as much as for strong interactions in the symmetry breaking sector of electroweak interactions.

## ACKNOWLEDGMENTS

We would like to thank Tao Han for useful discussions and use of his programs for  $b$  decay simulations. This research was supported in part by the University of Wisconsin Research Committee with funds granted by the Wisconsin Alumni Research Foundation and in part by the U. S. Department of Energy under Contract No. DE-FG02-95ER40896. The work of K.H. is supported in part by the JSPS-NSH Joint Research Project, and in part by Grant-in-Aid for Scientific Research from the Ministry of Education, Science and Culture of Japan. D.R. was supported in part by the NSF Summer Institute in Japan program.

## REFERENCES

- [1] For recent reviews, see e.g. J. L. Rosner, EFI-97-18, hep-ph/9704331; K.Hagiwara, Ann. Rev. Nucl. Part. Sci. 1998, 463; and references therein.
- [2] For recent reviews, see e.g. S. Dawson, hep-ph/9703387; M. Spira, Fortsch. Phys. **46**, 203 (1998); and references therein.
- [3] W. J. Marciano and F. E. Paige, Phys. Rev. Lett. **66**, 2433 (1991); J. F. Gunion, Phys. Lett. **B261**, 510 (1991).
- [4] A. Stange, W. Marciano, and S. Willenbrock, Phys. Rev. **D50**, 4491 (1994), [hep-ph/9404247]; R. Kleiss, Z. Kunszt, W. J. Stirling, Phys. Lett. **B253**, 269 (1991); H. Baer, B. Bailey, J. F. Owens, Phys. Rev. **D47**, 2730 (1993).
- [5] R. N. Cahn *et al.*, Phys. Rev. **D35**, 1626 (1987); V. Barger, T. Han, and R. J. N. Phillips, Phys. Rev. **D37**, 2005 (1988); R. Kleiss and W. J. Stirling, Phys. Lett. **200B**, 193 (1988); D. Froideveaux, in *Proceedings of the ECFA Large Hadron Collider Workshop*, Aachen, Germany, 1990, edited by G. Jarlskog and D. Rein (CERN report 90-10, Geneva, Switzerland, 1990), Vol II, p. 444; M. H. Seymour, *ibid*, p. 557; U. Baur and E. W. N. Glover, Nucl. Phys. **B347**, 12 (1990); Phys. Lett. **B252**, 683 (1990).
- [6] V. Barger, K. Cheung, T. Han, and R. J. N. Phillips, Phys. Rev. **D42**, 3052 (1990); V. Barger *et al.*, Phys. Rev. **D44**, 1426 (1991); V. Barger, K. Cheung, T. Han, and D. Zeppenfeld, Phys. Rev. **D44**, 2701 (1991); erratum Phys. Rev. **D48**, 5444 (1993); Phys. Rev. **D48**, 5433 (1993); V. Barger *et al.*, Phys. Rev. **D46**, 2028 (1992).
- [7] D. Dicus, J. F. Gunion, and R. Vega, Phys. Lett. **B258**, 475 (1991); D. Dicus, J. F. Gunion, L. H. Orr, and R. Vega, Nucl. Phys. **B377**, 31 (1991).
- [8] Y. L. Dokshitzer, V. A. Khoze, and S. Troyan, in *Proceedings of the 6th International Conference on Physics in Collisions*, (1986) ed. M. Derrick (World Scientific, 1987) p.365; J. D. Bjorken, Int. J. Mod. Phys. **A7**, 4189 (1992); Phys. Rev. **D47**, 101 (1993).

- [9] V. Barger, R. J. N. Phillips, and D. Zeppenfeld, Phys. Lett. **B346**, 106 (1995); K. Iordanidis and D. Zeppenfeld, Phys. Rev. **D57**, 3072 (1998), [hep-ph/9709506].
- [10] D. Cavalli *et al.*, ATLAS Internal Note PHYS-NO-051, Dec. 1994.
- [11] E. Richter-Was *et al.*, Int. J. Mod. Phys. **A13**, 1371 (1998).
- [12] W. W. Armstrong *et al.*, Atlas Technical Proposal, report CERN/LHCC/94-43 (1994); G. L. Bayatian *et al.*, CMS Technical Proposal, report CERN/LHCC/94-38 (1994).
- [13] V. Barger and R. J. N. Phillips, Phys. Rev. Lett. **55**, 2752 (1985); H. Baer, V. Barger, H. Goldberg, and R. J. N. Phillips, Phys. Rev. **D37**, 3152 (1988).
- [14] H. L. Lai *et al.*, Phys. Rev. **D55**, 1280 (1997), [hep-ph/9606399].
- [15] R. Cahn and S. Dawson, Phys. Lett. **136B**, 196 (1984).
- [16] D. Rainwater and D. Zeppenfeld, Journal of High Energy Physics 12, 005 (1997).
- [17] T. Han, G. Valencia and S. Willenbrock, Phys. Rev. Lett. **69**, 3274 (1992).
- [18] K. Hagiwara, A. D. Martin, and D. Zeppenfeld, Phys. Lett. **B235**, 198 (1990).
- [19] S. D. Ellis, R. Kleiss, and W. J. Stirling, Phys. Lett. **154B**, 435 (1985); R. Kleiss and W. J. Stirling, Nucl. Phys. **B262**, 235 (1985); Phys. Lett. **180B**, 171 (1986); J. F. Gunion, Z. Kunszt, and M. Soldate, Phys. Lett. **163B**, 389 (1985), Erratum, Phys. Lett. **168B**, 427 (1986); J. F. Gunion and M. Soldate, Phys. Rev. **D34**, 826 (1986); R. K. Ellis and R. J. Gonsalves, in *Proc. of the Workshop on super high energy physics*, Eugene, OR (1985), ed. D. E. Soper, p. 287.
- [20] K. Hagiwara and D. Zeppenfeld, Nucl. Phys. **B313**, 560 (1989).
- [21] V. Barger, T. Han and J. Ohnemus, and D. Zeppenfeld, Phys. Rev. Lett. **62**, 1971 (1989); Phys. Rev. **D40**, 2888 (1989).
- [22] F. A. Berends, W. T. Giele, H. Kuijf, R. Kleiss, and W. J. Stirling, Phys. Lett. **B224**, 237

(1989).

- [23] H. Chehime and D. Zeppenfeld, Phys. Rev. **D47**, 3898 (1993).
- [24] D. Rainwater, R. Szalapski, and D. Zeppenfeld, Phys. Rev. **D54**, 6680 (1996), [hep-ph/9605444].
- [25] F. A. Berends, H. Kuijf, B. Tausk, and W. T. Giele, Nucl. Phys. **B357**, 32 (1991).
- [26] V. Barger, E. Mirkes, R. J. N. Phillips, and T. J. Stelzer, Phys. Lett. **B338**, 336 (1994).
- [27] T. Stelzer and W. F. Long, Comp. Phys. Comm. **81**, 357 (1994), [hep-ph/9401258].
- [28] A. Stange, private communication.
- [29] R. K. Ellis *et al.*, Nucl. Phys. **B297**, 221 (1988).
- [30] B. K. Bullock, K. Hagiwara, and A. D. Martin, Phys. Lett. **B273**, 501 (1991); Nucl. Phys. **B395**, 499 (1993).